Inorganic Chemistry

pubs.acs.org/IC

Article

Activated Type I and Type II Process for Two-Photon Promoted ROS Generation: The Coordinated Zn Matters

Bo Ni,[#] Hongzhi Cao,[#] Chengkai Zhang, Shengli Li, Qiong Zhang, Xiaohe Tian, Dandan Li,* Jieying Wu, and Yupeng Tian*

Cite This: https://dx.doi.org/10.1021/acs.inorgchem.0c02030

Read Online

ACCESS | Metrics & More | Article Recommendations | Supporting Information

ABSTRACT: The construction of novel classes of photosensitizers for efficient reactive oxygen species (ROS) generation is of great interest, yet it is a challenge. In this work, a bis(terpyridine)zinc(II) complex (namely, **ZnL1**) with two-photon absorption activity as an efficient ROS photogenerator was synthesized. Benefiting from the coordinated Zn, the decreased singlet−triplet energy gap favors the intersystem crossing process facilitating the singlet oxygen ($^1O_2$) generation via energy transfer. In addition, it makes the superoxide radical ($O_2^{\bullet-}$) generation easier. This is an extremely rare study on two-photon excited ROS generation by activating type I and type II processes based on a cheaper and bioaccessible Zn complex.

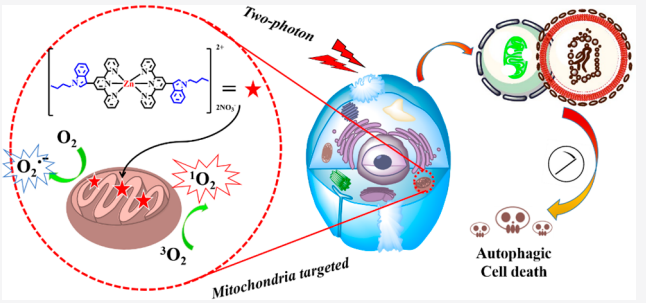

INTRODUCTION

Photodynamic therapy (PDT) is a novel cancer treatment method. It involves three important components, including photosensitizers (PSs), light, and oxygen. After irradiation, excited PSs interact with surrounding biomolecules or oxygen giving reactive oxygen species (ROS) to achieve the purpose of tumor treatment due to their key roles in cell signal transduction, cell multiplication, and homeostasis at a low level.[1,2] Typically, ROS are considered to be related to various pathological conditions and consist of the hydroxyl radical (OH·), hydrogen peroxide (H_2O_2), the superoxide radical ($O_2^{\bullet-}$), and singlet oxygen ($^1O_2$).[3−5] From these, the superoxide radical ($O_2^{\bullet-}$) and singlet oxygen ($^1O_2$) are the main and highly toxic reactive oxygen species, which are produced via electron transfer (type I mechanism) and energy transfer (type II mechanism) processes, respectively.[6] In particular, the search for photosensitizers (PSs) to achieve enhanced ROS production via both type I and type II processes is of pivotal interest.

To date, mostly reported PSs are organic molecules, including porphyrin, phthalocyanine, and their derivatives.[7] However, these molecules often have some inherent defects; one defect is that these materials are complex to synthesize and difficult to purify. In addition, most of them have a high self-aggregation tendency under physiological environments, leading to the decrease in fluorescence intensity. Also, their excitation wavelengths are mostly in the visible region; the damage to organisms is inevitable, which limits their utilization in living cells and tissue.[8−10] To address the above limitations, the use of metal complexes provides a promising platform for efficient ROS production and for the accompanied photodynamic therapy due to the simple preparation and their desirable photophysical properties, such as the well-studied Ru^{II}, Os^{II}, and Ir^{III} transition-metal complexes.[12−15] Meanwhile, the involved metal ions in these complexes are rare, which has always been a hurdle in cancer-targeting treatment due to their potential toxicity. Alternatively, the employed PS bearing heavy atoms can favor the intersystem crossing (ISC) process and boost the $^1O_2$ generation for potential PDT, which will involve disturbing dark toxicity as well.[16] In view of the specimen photodamage from traditional PSs, the newly emerging two-photon excited PDT provides an interesting alternative due to their near-infrared excitation source giving a larger penetration depth and weaker phototoxicity.[17,18]

Considering the above, we reasonably designed a D-A configuration bis(terpyridine)zinc(II) complex (**ZnL1**) without heavy atoms to fabricate a two-photon active material (Scheme 1). The results revealed that **ZnL1** exhibited considerable two-photon absorption activity in the near-infrared region. Of note, thanks to the coordination of Zn, its type I and type II processes for ROS generation has been activated, thus holding promise as a new strategy for efficient two-photon PDT.

Received: July 9, 2020

Downloaded via CORNELL UNIV on August 29, 2020 at 09:44:32 (UTC).
See https://pubs.acs.org/sharingguidelines for options on how to legitimately share published articles.

© XXXX American Chemical Society

Scheme 1. (a) Synthesis Route for New Complexes and (b) Schematic illustration of the Apoptosis Process Induced by Enhancement Type I and Type II Processes

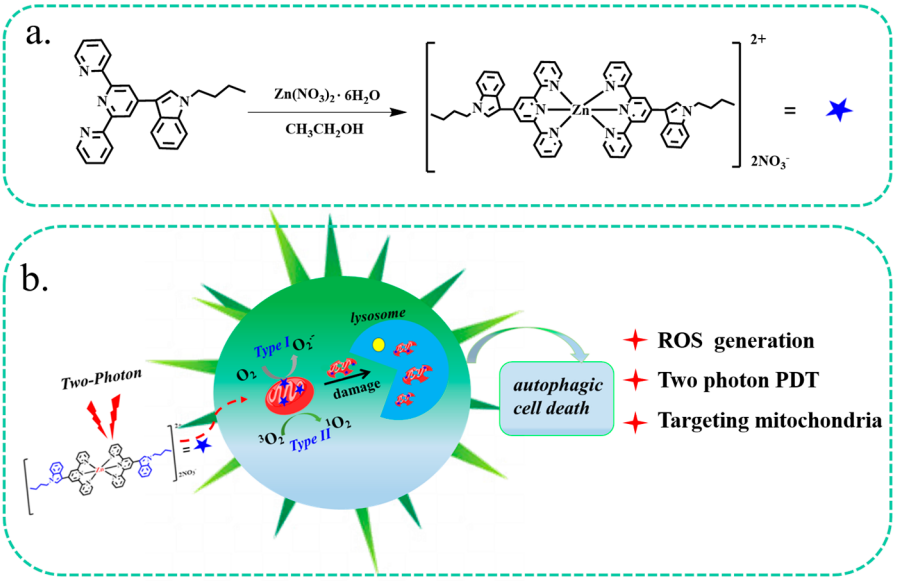

EXPERIMENTAL SECTION

Materials and Apparatuses. All chemicals for sample fabrication were purchased from Aladdin Industrial Corporation and purified by conventional methods. The apparatuses for sample characterization, single crystal structure, photophysical, and bioimaging relevant measurements in this work have been put into the Supporting Information in detail.

Computational Details. All calculations were recorded using the Gaussian 09 program, and the details for geometry optimization and relevant calculations were demonstrated in the Supporting Information.

Synthesis and Characterization. Synthesis of **L1**: To a solution of **N1** (1.0 g, 0.005 mol) in ethanol (60 mL) was added 2-acetylpyridine (1.22 g, 0.011 mol), KOH (1.17 g, 0.020 mol), and aqueous ammonia (60 mL, 30%). The reaction mixture was kept at 80 °C for 6 h. The precipitate formed after cooling and was collected by filtration. A yellow crystalline solid **L1** was obtained from recrystallization using ethanol. Yield, 64%. The single crystal of **L1** was grown from ethanol/dichloromethane solution. ^{1}H NMR (400 MHz, d_6-acetone, ppm): δ 8.99−8.82 (m, 6H), 8.19 (m, 1H), 8.12 (s, 1H), 8.03−7.90 (m, 2H), 7.62 (m, 1H), 7.52−7.36 (m, 2H), 7.35−7.16 (m, 2H), 4.50−4.28 (m, 2H), 1.53−1.33 (m, 2H), 1.20 (t, J = 7.1 Hz, 2H), 1.03−0.90 (m, 3H). ^{13}C NMR (100 MHz, d_6-DMSO): δ (ppm) 155.39, 155.30, 149.27, 145.11, 137.33, 136.98, 129.60, 125.14, 124.29, 122.06, 120.80, 120.74, 119.20, 116.86, 112.16, 110.97, 45.56, 40.13, 39.93, 39.72, 39.51, 39.30, 39.09, 38.88, 31.74, 19.50, 13.53. ESI−MS: calculated for $[M + H]^+$, 405.20; found, 405.20.

Synthesis of **ZnL1**: The ligand **L1** (0.4 g, 1.0 mmol) and $Zn(NO_3)_2{\cdot}6H_2O$ (0.18 g, 0.7 mmol) were dissolved in ethanol (50 mL), and the solution was heated under reflux with stirring for 3 h. Most of the ethanol was evaporated and cooled to room temperature, and red microcrystals are gradually precipitated. **ZnL1** was collected by filtration and washed with methanol. Yield, 68%. The single crystal of **ZnL1** was grown from methanol/chloroform solution. ^{1}H NMR (400 MHz, d_6-DMSO, ppm): δ 9.19 (s, 4H), 9.06 (d, J = 8.0 Hz, 4H), 8.85 (s, 2H), 8.52 (d, J = 4.6 Hz, 2H), 8.29 (t, J = 7.7 Hz, 4H), 7.97 (d, J = 4.8 Hz, 4H), 7.80 (d, J = 5.2 Hz, 2H), 7.57−7.47 (m, 4H), 7.47−7.33 (m, 4H), 4.43 (t, J = 6.7 Hz, 4H), 2.17−1.74 (m, 4H), 1.63−1.38 (m, 4H), 0.98 (t, J = 7.3 Hz, 6H). ^{13}C NMR (100 MHz, d_6-DMSO): δ 155.13, 149.82, 149.24, 148.36, 148.22, 148.00, 142.17, 141.82, 141.66, 137.34, 133.07, 130.59, 128.94, 128.72, 128.13, 127.90, 125.13, 123.75, 122.61, 120.72, 119.89, 113.34, 110.92, 45.83, 32.18, 19.93, 14.00. ESI−MS: calculated for [M], 996.30; found, 436.25. $[M\text{-}2NO_3^-]^{2+}/2$.

RESULTS AND DISCUSSION

Crystal Structures. Herein, the designed molecules with D-A configuration (Figure 1a) have been constructed, and the synthetic procedures were illustrated in Scheme S1. Figures S1−S9 displayed the detailed characterization data for intermediate and target products. The structural features of **L1** and **ZnL1** were analyzed by single crystal X-ray diffraction and shown in Figure 1b and Figure S10. Crystal structure shows that the C−C bonds between the indole ring and the electron acceptor (pyridine ring) of **L1** and **ZnL1** are 1.471 and 1.462 Å (**L1** > **ZnL1**), respectively, both of which are located between the normal C−C single bond and C═C double bond (Table S2). In addition, the dihedral angle between the electron donor indole quinary ring and the electron acceptor terpyridine moiety of **ZnL1** reveals that it is

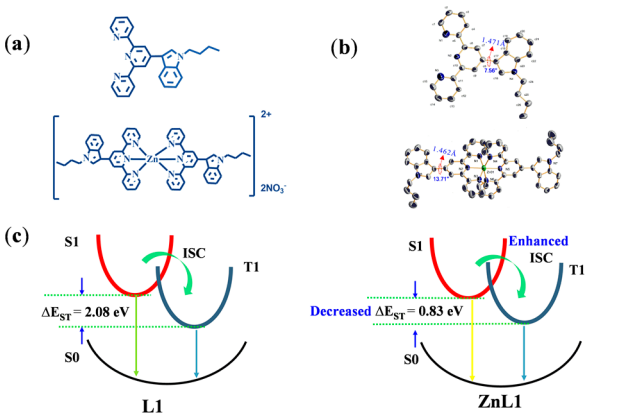

Figure 1. (a) Structural formulas of **L1** and **ZnL1**. (b) Crystal structures of **L1** and **ZnL1**; the displacement ellipsoids are drawn at the 30% probability level (for clarity, nitrate ions and H atoms within the molecules have been omitted). (c) The calculated ΔE_{ST} of **L1** and **ZnL1**.

https://dx.doi.org/10.1021/acs.inorgchem.0c02030
Inorg. Chem. XXXX, XXX, XXX−XXX

almost a planar structure. In this regard, the resultant enhanced electron delocalization and charge transfer within **ZnL1** will be conducive to its intensive two-photon activity.[11]

Photophysical Properties. Time-dependent density functional theory (TD-DFT) calculations are implemented to study the singlet−triplet energy gap (ΔE_{ST}) of **L1** and **ZnL1** (Figure S11). Evidently, the ΔE_{ST} values of **L1** and **ZnL1** are 2.08 and 0.83 eV (Figure 1c), respectively. The smaller ΔE_{ST} of **ZnL1** suggests its enhanced intersystem crossing (ISC) process favors the type II process, which gives the efficient $^1O_2$ generation.[19−22] Because the reduction of oxygen to superoxide would require the oxidation capacity of the zinc complex, the redox behavior of organic ligand **L1** and the corresponding complex **ZnL1** has been investigated. As shown in Figure S12, compared with that of **L1**, the lower oxidation potential of **ZnL1** (1.186 and 0.294 V for **L1** and **ZnL1**, respectively) makes the superoxide radical production (type I process) easier.

The UV−vis absorption spectra of **L1** and **ZnL1** are shown in Figure S13. By adjusting the electronic properties of the coordination metal, an absorption band located at 410 nm emerged (in DMSO) for **ZnL1** compared with that of **L1**, which belonged to the ligand-to-metal charge transfer (LMCT) process.[23] Also, the more abundant electron flow within **ZnL1** is beneficial to the type I process. The fluorescence behaviors of the **L1**/**ZnL1** were measured in different solvents (Figure S13 and Table S3). Upon the excitation at the maximum absorption wavelength, they exhibit similar emission wavelengths. Interestingly, the fluorescence quantum yield of **ZnL1** was significantly lower than that in **L1** in different solvents which may be due to the nature of competition between the ISC (S_1−T_1) and fluorescence decay (S_1−S_0) (Figure S14).[16] For **ZnL1**, given its smaller ΔE_{ST}, most of the S_1 excitons convert into the T_1 state favoring the ROS generation instead of fluorescent emission. The stability of **ZnL1** in PBS buffers was also checked (Figures S15 and S16). Obviously, as shown in Figure S18a, **ZnL1** showed long-lived excited states with respect to those of **L1** (4.25 and 7.24 ns for **L1** and **ZnL1**, respectively), which is conducive to the ISC process favoring $^1O_2$ generation (activated type II process).[24,25]

We, herein, demonstrated that increased electron delocalization and charge transfer within **ZnL1** would strengthen its two-photon absorption activity (Figure S17). Frankly, the results unveiled that the two-photon absorption cross section of **ZnL1** was enhanced 1.21 times that of **L1** in the wavelength range from 680 to 900 nm (Figure 2a).

Light Triggered $^1O_2$ and $O_2^{\bullet-}$ Generation. The above results motivated us to study the ROS generation ability of **L1** and **ZnL1**. Therefore, 2′,7′-dichlorodihydrofluorescein diacetate (H_2DCF-DA), as an ROS indicator with a lighting-on signal (green-emitting centered at 525 nm) when reacting with ROS, was used to detect the ROS generation level of **L1** and **ZnL1**. After H_2DCF-DA was mixed with **L1**/**ZnL1**, upon illumination, the green-emitting signal of H_2DCF-DA increased significantly, which showed that **L1**/**ZnL1** could produce effective reactive oxygen species.[26−28] At the same time, after 10 min of irradiation, it was found that the fluorescence intensity of **ZnL1** was 2.17 times higher than that of **L1** (Figure S18c,d). This indicated that the capacity of **ZnL1** to generate reactive oxygen species was significantly higher than that of **L1**. Furthermore, electron spin resonance (ESR) trapping measurements were carried out to further

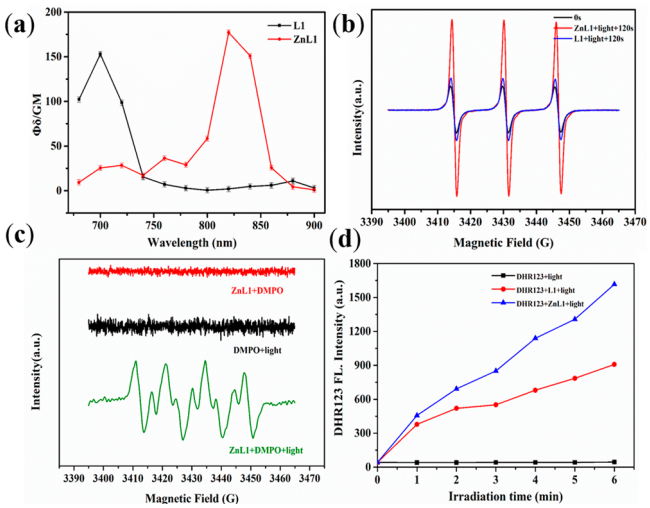

Figure 2. (a) Two-photon (TP) action cross section of **L1** and **ZnL1** (excitation wavelength = 680−900 nm, identical energy = 500 mW). (b) ESR signals of **L1**/**ZnL1** trapped by TEMP with and without light irradiation (c = 10 μM). (c) ESR signals of **ZnL1** trapped by DMPO with and without light irradiation. (d) The increasing fluorescence intensity of DHR123 (526 nm) in **L1** and **ZnL1** solution (10 μM) under light irradiation within 6 min ($c = 1 \times 10^{-5}$ mol/L, λ_{ex} = 410 nm, EX slit = 5.0 nm, EM slit = 5.0 nm).

distinguish the photogenerated ROS species. Accordingly, 2,2,6,6-tetramethylpiperidine (TEMP) and 5,5-dimethyl-1-pyrroline-*N*-oxide (DMPO) were added into the targeted systems (**L1** and **ZnL1**) to trap as the $^1O_2$ and $O_2^{\bullet-}$ trapping agents, respectively. As illustrated in Figure 2b, characteristic signals of 4-oxo-TEMPO (g = 2.0055, 1:1:1 triplet) under light irradiation for **L1** and **ZnL1** were displayed, manifesting the production of $^1O_2$. In addition, the stronger signals of **ZnL1** reveal its enhanced ISC behavior as a result of the smaller ΔE_{ST}. As shown in Figure 2c, no obviously ESR signals could be observed for **ZnL1** in the dark.[29−31] In addition, in contrast to the negligible signals of the **L1** system (Figure S19a), accordant signals with DMPO−OOH as a spin derivative of DMPO−$O_2^{\bullet-}$ were obtained for **ZnL1**, suggesting it has the ability to reduce O_2 to $O_2^{\bullet-}$ species. The above results elaborated that, thanks to the coordinated Zn atoms, **ZnL1** can effectively produce singlet oxygen and superoxide radicals. Moreover, as shown in Figures S19b,c and S20 and Figure 2d, the generated ROS were further confirmed by the probe 9,10-anthracenedipropanoic acid (ABDA) and the $O_2^{\bullet-}$ probe dihydrorhodamine 123 (DHR123). The production efficiencies of $^1O_2$ by **L1**/**ZnL1** were determined using ABDA as the $^1O_2$ indicator. As we expected, their relative $^1O_2$ quantum yields (Φps) showed different values (0.09 and 0.72 for **L1** and **ZnL1**, respectively) when using Rose Bengal (RB) (Φ_{RB} = 0.75 in H_2O) as the standard under cell-free conditions (respectively, see Figures S20 and S21).[20]

Intracellular ROS Detection. Benefiting from the high-performance of **ZnL1** in producing ROS in vitro, the study to evaluate the ROS generation of **ZnL1** inside HeLa cells was carried out next.[6,32] HeLa cells were incubated with both **ZnL1** and 2′,7′-dichlorofluorescein diacetate (DCFH-DA); herein, DCFH-DA was used as an intracellular ROS indicator. Then, the resulting cells were exposed to 830 nm of light irradiation (100 mW/cm^2), and then, the confocal laser scanning microscopy (CLSM) images were collected during incubation time. As shown in Figure 3a, the green fluorescent signals of

https://dx.doi.org/10.1021/acs.inorgchem.0c02030
Inorg. Chem. XXXX, XXX, XXX−XXX

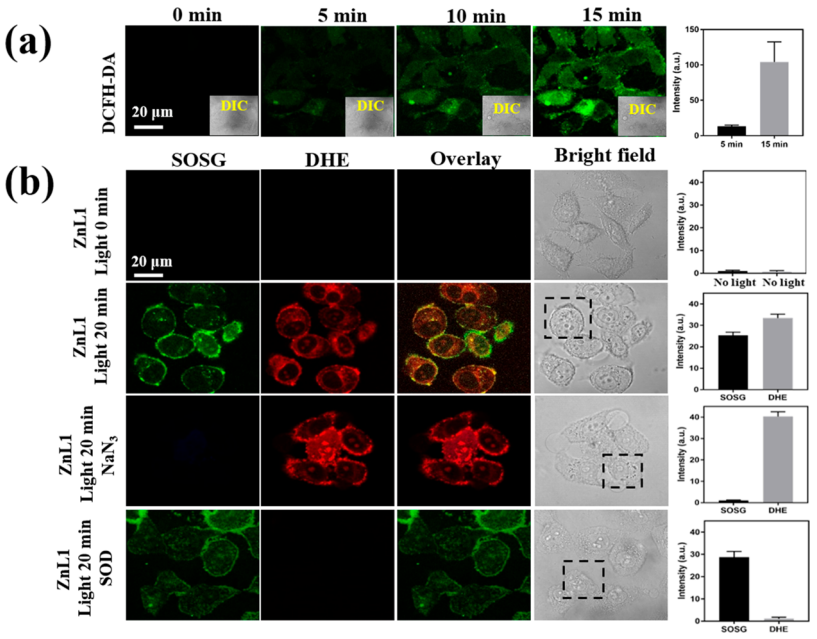

Figure 3. (a) CLSM images of HeLa cells treated with DCFH-DA (λ_{ex} = 488 nm, λ_{em} = 510−540 nm) followed by the incubation of **ZnL1** (10 μM), respectively (two-photon light irradiation = 830 nm, 100 mW/cm^2). Scale bar: 20 μm. (b) ROS detection in HeLa cells using DHE and SOSG as the $O_2^{\cdot-}$ and $^1O_2$ probes, respectively. NaN_3 and SOD as the specific scavengers for $^1O_2$ and $O_2^{\cdot-}$, respectively (the boxes in the bright field represent the morphology of cells under different conditions). Scale bar: 20 μm.

DCFH-DA demonstrated that cells treated with **ZnL1** exhibited effective ROS generation upon light irradiation. Moreover, the ROS were also studied using standard dihydroethidium (DHE) and singlet oxygen sensor green (SOSG) staining methods.[23,33] As shown in Figure 3b, after exposure to the 830 nm laser light, the bright red fluorescence of DHE and the green fluorescence of SOSG were observed in HeLa cells by CLSM. In addition, NaN_3 and superoxide dismutase (SOD), applied as the specific scavengers for $^1O_2$ and $O_2^{\cdot-}$, were added into the above system. Obviously, NaN_3 and SOD dramatically decreased DHE/SOSG oxidation in the **ZnL1** system. These results demonstrated that the Zn complex can generate singlet oxygen and superoxide radicals by photoactivation.

ROS Production Mechanisms. In view of the above results, we proposed that the pathway of ROS production for **ZnL1** under two-photon excitation is as follows (Figure 4): During this process, a photosensitizer (**ZnL1**) absorbs two near-infrared photons, is excited to the singlet states (^{1}**ZnL1**) from its ground states (S_0), and then undergoes the ISC process to produce the longer-lived triplet states (^{3}**ZnL1**). In the type I process, ^{3}**ZnL1** can react with the biological environment through the electron transfer mechanism to produce $O_2^{\cdot-}$ radicals. Meanwhile, for the type II process, the energy of the excited ^{3}**ZnL1** is transferred to molecular oxygen (O_2) to generate singlet oxygen ($^1O_2$). These species are highly reactive and can trigger cell death resulting from the direct reaction with the biological surroundings.[34−36]

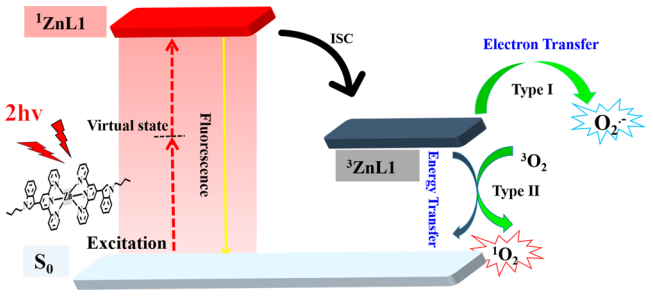

Figure 4. Schematic illustration of $^1O_2$ generation through the energy transfer process and $O_2^{\cdot-}$ generation through the electron transfer process.

Cellular Localization. Considering the excellent 2PA and efficient ROS activities of **ZnL1**, the biological imaging application of **ZnL1** was carried out using HeLa cells. First, HeLa cells were incubated with **ZnL1** (10 μM) for 15 min. It can be found that **ZnL1** penetrated the cell membrane and distinct mitochondrial location well (Figure 5a and Figure S24a).[36] To further test the mitochondria-targeting property of **ZnL1**, the colocalization imaging experiment using **ZnL1** and MitoTracker Red (a red fluorescent dye that targets mitochondria) to colabel HeLa cells was performed. As illustrated in Figure 5b, the distribution of **ZnL1** in cells was consistent with that of MitoTracker Red (Pearson's colocalization coefficient value is 0.95),[37] which demonstrated that **ZnL1** can specifically localize to mitochondria in HeLa cells. As reported, the mitochondria-targeting ability of **ZnL1** can be ascribed to its moderate hydrophobicity (log P = 0.26) and cationic feature (Figure S22).[38,39]

In Vitro Anticancer Activities and PDT Activities. Encouraged by the efficient ROS generation and desirable two-photon activity of **ZnL1**, we conducted a preliminary test on its ability to induce apoptosis. First, an MTT method was carried out to evaluate the PDT efficacy of **ZnL1** in vitro. As shown in Figure S23, **L1** and **ZnL1** displayed negligible dark cytotoxicity (over 85% of the cells are alive at a concentration of 10 μM). For photocytotoxicity measurement, HeLa cells were treated with **L1**/**ZnL1** (10 μM) and exposed to the light. Interestingly, in contrast that of **L1**, only about 20% of treated cells survived for **ZnL1**. This indicated that **ZnL1** exhibited comparable PDT efficacy in vitro. The PDT effect of **ZnL1** was also

https://dx.doi.org/10.1021/acs.inorgchem.0c02030
Inorg. Chem. XXXX, XXX, XXX−XXX

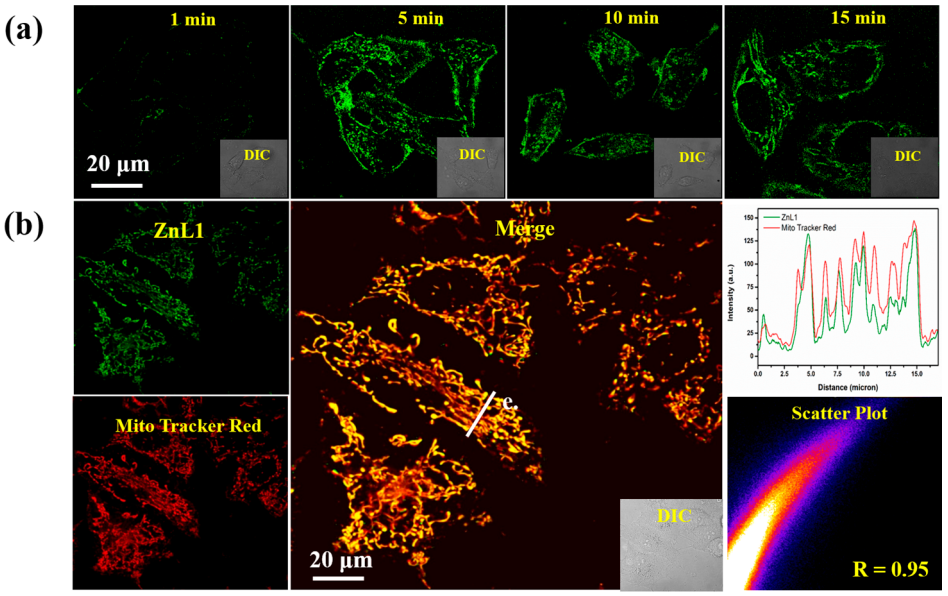

Figure 5. (a) CLSM images of HeLa cells treated with **ZnL1** (10 μM) in aqueous phosphate buffered saline (PBS) buffer at different times. (b) Determination of intercellular localization of **ZnL1** by confocal microscopy in HeLa cells. Colocalization images of HeLa cells stained with MitoTracker Red (0.5 μM, red channel, λ_{ex} = 534 nm, λ_{em} = 600 ± 20 nm) and **ZnL1** (10 μM, green channel, λ_{ex} = 410 nm, λ_{em} = 480 ± 20 nm), with the fluorescence intensity of the line in the merged image and colocalization coefficient. Scale bar: 20 μm.

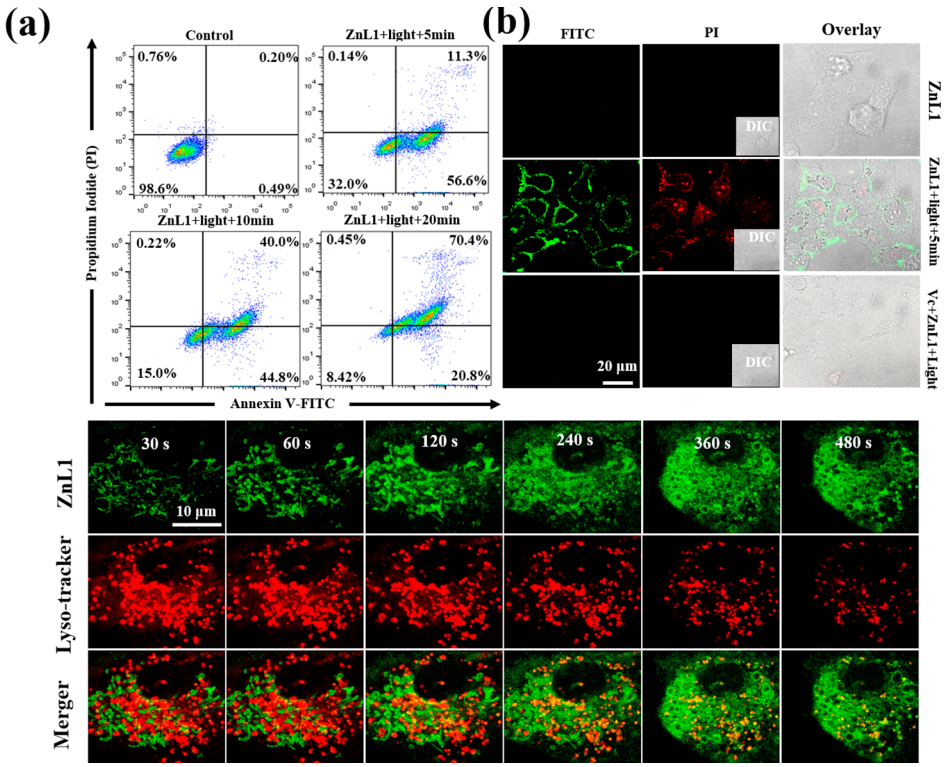

Figure 6. (a) Flow cytometry quantification of Annexin V-FITC and propidium iodide (PI) labeled HeLa cells. The cells were treated with **ZnL1** (10 μM) for 12 h before being irradiated. Light group: Cells were processed with light irradiation after treatment with **ZnL1** for different amounts of time (830 nm, 100 mW/cm^2). (b) PDT efficacy of **ZnL1** (10 μM) in vitro using Annexin V-FITC/PI (5 μM) treatment (without light irradiation). HeLa cells in vitro after different treatments. **ZnL1** incubated with Annexin V-FITC and under PI (830 nm, 100 mW/cm^2, 15 min). Scale bar: 20 μm. (c) CLSM images of HeLa cells treated by Lyso-tracker Green (1 μM, λ_{ex} = 488 nm, λ_{em} = 490−520 nm) and **ZnL1** (10 μM) with different irradiation times (1−6 min). Scale bar: 10 μm.

researched using the flow cytometry cell apoptosis assay to detect cell apoptosis before and after irradiation.[5,33] As shown in Figure 6a, compared with the dark condition, upon light irradiation at different times, **ZnL1** resulted in 70.4% apoptosis; these results showed high apoptosis enhancement under light by **ZnL1.** In addition, we also performed the Annexin V-FITC/PI experiment to study the PDT efficiency. As shown in Figure 6b, after HeLa cells were incubated with 10

https://dx.doi.org/10.1021/acs.inorgchem.0c02030
Inorg. Chem. XXXX, XXX, XXX−XXX

μM **ZnL1** for 15 min and then stained with Annexin V-FITC/PI, ignorable apoptosis signals could be observed without irradiation. On the contrary, in the PDT group, the red and green fluorescence intensity signals were detected which indicated that **ZnL1** could induce cancer cell apoptosis under 830 nm of light irradiation. Considering the positively charged character of **ZnL1**, its mitochondria-targeting ability will play a vital role in cell apoptosis due to the fact that mitochondria are the main place where cells produce energy, and mitochondrial damage can easily lead to apoptosis.[40,41] Then, we further studied the behavior of **ZnL1** in living cells to detect the process of cell damage in real time under 830 nm excitation. It was found that **ZnL1** could target mitochondria well, and the time-resolved imaging with lysosomes showed that the cell morphology gradually shrank; the filamentous mitochondria gradually became punctate after 120 s, which meant that mitochondria began autophagy (Figure 6c). About 360 s later, mitochondria and lysosomes began autophagy. Lysosomes fuse continuously and eventually form apoptotic vesicles, leading to apoptosis (Figure S24c).[33,42] According to the above results, the **ZnL1** in our work exhibits good photostability, multiple ROS types, high singlet oxygen quantum yields, low dark toxicity, and moderate excitation wavelengths (Table S5). It demonstrated that **ZnL1** could be employed as an efficient two-photon excited ROS generator for potentially photodynamic therapy.

CONCLUSIONS

In summary, we have rationally designed and fabricated a noble-metal-free bis(terpyridine)zinc(II) complex (**ZnL1**) bearing two-photon activity. Thanks to the coordination of the Zn atom, the involved electron transfer (type I) and energy transfer (type II) processes for ROS generation have been activated. Moreover, based on the characteristics of cationic and lipophilic compounds, **ZnL1** has outstanding mitochondria-targeting ability. Flow cytometry assay showed that **ZnL1** could significantly enhance the anticancer activity under two-photon light irradiation. These results clarify that **ZnL1** can produce ROS upon light irradiation and then cause the cell death. Overall, this work provides a new platform for switching on two-photon excited ROS generation without the introduction of heavy atoms.

ASSOCIATED CONTENT

Supporting Information

The Supporting Information is available free of charge at https://pubs.acs.org/doi/10.1021/acs.inorgchem.0c02030.

General experimental details, synthetic procedures, characterization data, crystal structure, optical physical data, ROS detection, HNMR sprectra, CNMR spectra, mass spectra, ORTEP structures, HOMO and LUMO distributions, cyclic voltammetry (CV), UV−vis absorption spectra, quantum yield, time evolution of UV−vis absorption spectra, stability of complexes, two-photon fluorescence intensity, fluorescence lifetime spectra, ESR signals, chemical trapping measurements, decomposition rate constants, octanol/water partition coefficient, HeLa cell toxicity data, single photon confocal development, crystal data and structure refinement, selected bond lengths, photophysical data, dark toxicity and phototoxicity, and coordinates of the atoms (PDF)

Accession Codes

CCDC 1919752 and 1959885 contain the supplementary crystallographic data for this paper. These data can be obtained free of charge via www.ccdc.cam.ac.uk/data_request/cif, or by emailing data_request@ccdc.cam.ac.uk, or by contacting The Cambridge Crystallographic Data Centre, 12 Union Road, Cambridge CB2 1EZ, UK; fax: +44 1223 336033.

AUTHOR INFORMATION

Corresponding Authors

Dandan Li − *Institutes of Physics Science and Information Technology, Key Laboratory of Structure and Functional Regulation of Hybrid Materials, Ministry of Education, Anhui University, Hefei 230601, P. R. China;* orcid.org/0000-0002-3504-8739; Email: chemlidd@163.com

Yupeng Tian − *Department of Chemistry, Key Laboratory of Functional Inorganic Material Chemistry of Anhui Province, Anhui University, Hefei 230601, P. R. China*; Email: yptian@ahu.edu.cn

Authors

Bo Ni − *Institutes of Physics Science and Information Technology, Key Laboratory of Structure and Functional Regulation of Hybrid Materials, Ministry of Education and Department of Chemistry, Key Laboratory of Functional Inorganic Material Chemistry of Anhui Province, Anhui University, Hefei 230601, P. R. China*

Hongzhi Cao − *School of Life Science, Anhui University, Hefei 230601, P. R. China*

Chengkai Zhang − *Department of Chemistry, Key Laboratory of Functional Inorganic Material Chemistry of Anhui Province, Anhui University, Hefei 230601, P. R. China*

Shengli Li − *Department of Chemistry, Key Laboratory of Functional Inorganic Material Chemistry of Anhui Province, Anhui University, Hefei 230601, P. R. China*

Qiong Zhang − *Department of Chemistry, Key Laboratory of Functional Inorganic Material Chemistry of Anhui Province, Anhui University, Hefei 230601, P. R. China*

Xiaohe Tian − *School of Life Science, Anhui University, Hefei 230601, P. R. China;* orcid.org/0000-0002-2294-3945

Jieying Wu − *Department of Chemistry, Key Laboratory of Functional Inorganic Material Chemistry of Anhui Province, Anhui University, Hefei 230601, P. R. China*

Complete contact information is available at: https://pubs.acs.org/10.1021/acs.inorgchem.0c02030

Author Contributions

#B.N and H.Z.C. contributed equally to this work.

Notes

The authors declare no competing financial interest.

ACKNOWLEDGMENTS

This work was supported by grants for the National Natural Science Foundation of China (21871003, 21701160, 51672002, and 51772002), Doctor Start-up Fund (S020118002/026), Hefei National Laboratory for Physical Sciences at the Microscale (KF2019002), and Natural Science Foundation of Anhui Province of China (1908085MB30).

REFERENCES

(1) Dolmans, D. E.; Fukumura, D.; Jain, R. K. Photodynamic therapy for cancer. *Nat. Rev. Cancer* **2003**, *3*, 380−387.

(2) Bonnett, R. Photosensitizers of the porphyrin and phthalocyanine series for photodynamic therapy. *Chem. Soc. Rev.* **1995**, *24*, 19−33.
(3) Lan, M.; Zhao, S.; Liu, W.; Lee, C. S.; Zhang, W.; Wang, P. Photosensitizers for photodynamic therapy. *Adv. Healthcare Mater.* **2019**, *8*, 1900132.
(4) Awuah, S. G.; You, Y. Boron dipyrromethene (BODIPY)-based photosensitizers for photodynamic therapy. *RSC Adv.* **2012**, *2*, 11169−11183.
(5) Dai, Y.; Yang, Z.; Cheng, S.; Wang, Z.; Zhang, R.; Zhu, G.; Wang, Z.; Yung, B. C.; Tian, R.; Jacobson, O.; et al. Toxic Reactive Oxygen Species Enhanced Synergistic Combination Therapy by Self-Assembled Metal-Phenolic Network Nanoparticles. *Adv. Mater.* **2018**, *30*, 1704877.
(6) Monro, S.; Colón, K. L.; Yin, H.; Roque, J., III; Konda, P.; Gujar, S.; Thummel, R. P.; Lilge, L.; Cameron, C. G.; McFarland, S. A. Transition metal complexes and photodynamic therapy from a tumor-centered approach: Challenges, opportunities, and highlights from the development of TLD1433. *Chem. Rev.* **2019**, *119*, 797−828.
(7) DeRosa, M. C.; Crutchley, R. Photosensitized singlet oxygen and its applications. *Coord. Chem. Rev.* **2002**, *233*, 351−371.
(8) Sun, Z.; Zhang, L. P.; Wu, F.; Zhao, Y. Photosensitizers for Two-Photon Excited Photodynamic Therapy. *Adv. Funct. Mater.* **2017**, *27*, 1704079.
(9) Kim, H. M.; Jung, C.; Kim, B. R.; Jung, S. Y.; Hong, J. H.; Ko, Y. G.; Lee, K. J.; Cho, B. R. Environment-sensitive two-photon probe for intracellular free magnesium ions in live tissue. *Angew. Chem., Int. Ed.* **2007**, *46*, 3460−3463.
(10) Lim, C. S.; Masanta, G.; Kim, H. J.; Han, J. H.; Kim, H. M.; Cho, B. R. Ratiometric detection of mitochondrial thiols with a two-photon fluorescent probe. *J. Am. Chem. Soc.* **2011**, *133*, 11132−11135.
(11) Li, D.; Li, B.; Wang, S.; Zhang, C.; Cao, H.; Tian, X.; Tian, Y. Modification of side chain of conjugated molecule for enhanced charge transfer and two-photon activity. *Spectrochim. Acta, Part A* **2020**, *224*, 117448.
(12) Huang, H.; Yu, B.; Zhang, P.; Huang, J.; Chen, Y.; Gasser, G.; Ji, L.; Chao, H. Highly Charged Ruthenium (II) Polypyridyl Complexes as Lysosome-Localized Photosensitizers for Two-Photon Photodynamic Therapy. *Angew. Chem., Int. Ed.* **2015**, *54*, 14049−14052.
(13) Jakubaszek, M.; Goud, B.; Ferrari, S.; Gasser, G. Mechanisms of action of Ru (II) polypyridyl complexes in living cells upon light irradiation. *Chem. Commun.* **2018**, *54*, 13040−13059.
(14) Sun, Y.; Joyce, L. E.; Dickson, N. M.; Turro, C. DNA photocleavage by an osmium (II) complex in the PDT window. *Chem. Commun.* **2010**, *46*, 6759−6761.
(15) Novohradsky, V.; Rovira, A.; Hally, C.; Galindo, A.; Vigueras, G.; Gandioso, A.; Svitelova, M.; Bresolí-Obach, R.; Kostrhunova, H.; Markova, L.; et al. Towards Novel Photodynamic Anticancer Agents Generating Superoxide Anion Radicals: A Cyclometalated Ir^{III} Complex Conjugated to a Far-Red Emitting Coumarin. *Angew. Chem., Int. Ed.* **2019**, *58*, 6311−6315.
(16) Xiao, Y.-F.; Chen, J.-X.; Li, S.; Tao, W.-W.; Tian, S.; Wang, K.; Cui, X.; Huang, Z.; Zhang, X.-H.; Lee, C.-S. Manipulating exciton dynamics of thermally activated delayed fluorescence materials for tuning two-photon nanotheranostics. *Chem. Sci.* **2020**, *11*, 888−895.
(17) Starkey, J.; Rebane, A.; Drobizhev, M.; Meng, F.; Gong, A.; Elliott, A.; McInnerney, K.; Spangler, C. New two-photon activated photodynamic therapy sensitizers induce xenograft tumor regressions after near-IR laser treatment through the body of the host mouse. *Clin. Cancer Res.* **2008**, *14*, 6564−6573.
(18) Chen, R.; Zhang, J.; Chelora, J.; Xiong, Y.; Kershaw, S. V.; Li, K. F.; Lo, P.-K.; Cheah, K. W.; Rogach, A. L.; Zapien, J. A.; Lee, C.-S. Ruthenium (II) Complex Incorporated UiO-67 Metal−Organic Framework Nanoparticles for Enhanced Two-Photon Fluorescence Imaging and Photodynamic Cancer Therapy. *ACS Appl. Mater. Interfaces* **2017**, *9*, 5699−5708.
(19) Li, C.; Ren, Z.; Yan, S. Thermally activated delayed fluorescence materials in OLEDs devices: Design, synthesis and applications. *Kexue Tongbao* **2015**, *60*, 2989−3004.
(20) Zhang, C.; Zhao, Y.; Li, D.; Liu, J.; Han, H.; He, D.; Tian, X.; Li, S.; Wu, J.; Tian, Y. Aggregation-induced emission (AIE)-active molecules bearing singlet oxygen generation activities: the tunable singlet-triplet energy gap matters. *Chem. Commun.* **2019**, *55*, 1450−1453.
(21) An, Z.; Zheng, C.; Tao, Y.; Chen, R.; Shi, H.; Chen, T.; Wang, Z.; Li, H.; Deng, R.; Liu, X.; Huang, W. Stabilizing triplet excited states for ultralong organic phosphorescence. *Nat. Mater.* **2015**, *14*, 685−690.
(22) Li, J.-A.; Zhou, J.; Mao, Z.; Xie, Z.; Yang, Z.; Xu, B.; Liu, C.; Chen, X.; Ren, D.; Pan, H.; Shi, G.; Zhang, Y.; Chi, Z. Transient and Persistent Room-Temperature Mechanoluminescence from a White-Light-Emitting AIEgen with Tricolor Emission Switching Triggered by Light. *Angew. Chem., Int. Ed.* **2018**, *57*, 6449−6453.
(23) Li, M.; Xia, J.; Tian, R.; Wang, J.; Fan, J.; Du, J.; Long, S.; Song, X.; Foley, J. W.; Peng, X. Near-infrared light-initiated molecular superoxide radical generator: rejuvenating photodynamic therapy against hypoxic tumors. *J. Am. Chem. Soc.* **2018**, *140*, 14851−14859.
(24) Mao, Z.; Yang, Z.; Fan, Z.; Ubba, E.; Li, W.; Li, Y.; Zhao, J.; Yang, Z.; Aldred, M. P.; Chi, Z. The methylation effect in prolonging the pure organic room temperature phosphorescence lifetime. *Chem. Sci.* **2019**, *10*, 179−184.
(25) Yang, Z.; Mao, Z.; Zhang, X.; Ou, D.; Mu, Y.; Zhang, Y.; Zhao, C.; Liu, S.; Chi, Z.; Xu, J.; Wu, Y.-C.; Lu, P.-Y.; Lien, A.; Bryce, M. R. Intermolecular Electronic Coupling of Organic Units for Efficient Persistent Room-Temperature Phosphorescence. *Angew. Chem., Int. Ed.* **2016**, *55*, 2181−2185.
(26) Apel, K.; Hirt, H. Reactive oxygen species: metabolism, oxidative stress, and signal transduction. *Annu. Rev. Plant Biol.* **2004**, *55*, 373−399.
(27) Andreyev, A.; Kushnareva, Y.; Starkov, A. Mitochondrial metabolism of reactive oxygen species. *Biochemistry (Moscow)* **2005**, *70*, 200−214.
(28) Zheng, Z.; Zhang, T.; Liu, H.; Chen, Y.; Kwok, R. T. K.; Ma, C.; Zhang, P.; Sung, H. H. Y.; Williams, I. D.; Lam, J. W. Y.; Wong, K. S.; Tang, B. Z. Bright near-infrared aggregation-induced emission luminogens with strong two-photon absorption, excellent organelle specificity, and efficient photodynamic therapy potential. *ACS Nano* **2018**, *12*, 8145−8159.
(29) Li, M.; Xia, J.; Tian, R.; Wang, J.; Fan, J.; Du, J.; Long, S.; Song, X.; Foley, J. W.; Peng, X. Near-infrared light-initiated molecular superoxide radical generator: rejuvenating photodynamic therapy against hypoxic tumors. *J. Am. Chem. Soc.* **2018**, *140*, 14851−14859.
(30) Buettner, G. The Spin Trapping of Superoxide and Hydroxyl Free Radicals with DMPO (5,5-Dimethylpyrroline-N-oxide): More About Iron. *Free Radical Res. Commun.* **1993**, *19*, No. s79-s87.
(31) Chen, Y.; Wang, Z.; Wang, H.; Lu, J.; Yu, S.; Jiang, H. Singlet Oxygen-Engaged Selective Photo-Oxidation over Pt Nanocrystals/Porphyrinic MOF: The Roles of Photothermal Effect and Pt Electronic State. *J. Am. Chem. Soc.* **2017**, *139*, 2035−2044.
(32) Li, X.; Wu, J.; Wang, L.; He, C.; Chen, L.; Jiao, Y.; Duan, C. Mitochondrial-DNA-Targeted Ir(III)-Containing Metallohelices with Tunable Photodynamic Therapy Efficacy in Cancer Cells. *Angew. Chem.* **2020**, *132* (16), 6482−6489.
(33) Novohradsky, V.; Vigueras, G.; Pracharova, J.; Cutillas, N.; Janiak, C.; Kostrhunova, H.; Brabec, V.; Ruiz, J.; Kasparkova, J. Molecular superoxide radical photogeneration in cancer cells by dipyridophenazine iridium (iii) complexes. *Inorg. Chem. Front.* **2019**, *6*, 2500−2513.
(34) Liu, J.; Bu, W.; Shi, J. Chemical design and synthesis of functionalized probes for imaging and treating tumor hypoxia. *Chem. Rev.* **2017**, *117*, 6160−6224.
(35) Zhou, Z.; Song, J.; Nie, L.; Chen, X. Reactive oxygen species generating systems meeting challenges of photodynamic cancer therapy. *Chem. Soc. Rev.* **2016**, *45*, 6597−6626.

https://dx.doi.org/10.1021/acs.inorgchem.0c02030
Inorg. Chem. XXXX, XXX, XXX−XXX

(36) Zhang, L.; Li, Y.; Che, W.; Zhu, D.; Li, G.; Xie, Z.; Song, N.; Liu, S.; Tang, B.; Liu, X.; Su, Z.; Bryce, M. AIE Multinuclear Ir(III) Complexes for Biocompatible Organic Nanoparticles with Highly Enhanced Photodynamic Performance. *Adv. Sci.* **2019**, *6*, 1802050.
(37) Huang, H.; Tian, Y. A ratiometric fluorescent probe for bioimaging and biosensing of HBrO in mitochondria upon oxidative stress. *Chem. Commun.* **2018**, *54*, 12198−12201.
(38) Horobin, R. W.; Stockert, J. C.; Rashid-Doubell, F. Fluorescent cationic probes for nuclei of living cells: why are they selective? A quantitative structure−activity relations analysis. *Histochem. Cell Biol.* **2006**, *126*, 165−175.
(39) Feng, Z.; Li, D.; Zhang, M.; Shao, T.; Shen, Y.; Tian, X.; Zhang, Q.; Li, S.; Wu, J.; Tian, Y. Enhanced three-photon activity triggered by the AIE behaviour of a novel terpyridine-based Zn(II) complex bearing a thiophene bridge. *Chem. Sci.* **2019**, *10* (30), 7228−7232.
(40) Oleinick, N.; Morris, R.; Belichenko, I. The role of apoptosis in response to photodynamic therapy: what, where, why, and how. *Photochem. Photobiol. Sci.* **2002**, *1*, 1−21.
(41) Li, Y.; Wu, X.; Liu, X.; Li, P. Mitophagy imbalance in cardiomyocyte ischaemia/reperfusion injury. *Acta Physiol.* **2019**, *225*, No. e13228.
(42) Jung, H. S.; Han, J.; Lee, J.-H.; Lee, J. H.; Choi, J.-M.; Kweon, H.-S.; Han, J. H.; Kim, J.-H.; Byun, K. M.; Jung, J. H.; Kang, C.; Kim, J. S. Enhanced NIR radiation-triggered hyperthermia by mitochondrial targeting. *J. Am. Chem. Soc.* **2015**, *137*, 3017−3023.

https://dx.doi.org/10.1021/acs.inorgchem.0c02030
Inorg. Chem. XXXX, XXX, XXX−XXX